Buoyant Low Stretch Diffusion Flames Beneath Cylindrical PMMA Samples

by
S. L. Olson
NASA Lewis Research Center
and
J. S. T'ien
Case Western Reserve University

Abstract

A unique new way to study low gravity flames in normal gravity has been developed. To study flame structure and extinction characteristics in low stretch environments, a normal gravity low-stretch diffusion flame is generated using a cylindrical PMMA sample of varying large radii. Burning rates, visible flame thickness, visible flame standoff distance, temperature profiles in the solid and gas, and radiative loss from the system were measured. A transition from the blowoff side of the flammability map to the quenching side of the flammability map is observed at approximately 6-7 sec^{-1}, as determined by curvefits to the non-monotonic trends in peak temperatures, solid and gas-phase temperature gradients, and non-dimensional standoff distances. A surface energy balance reveals that the fraction of heat transfer from the flame that is lost to in-depth conduction and surface radiation increases with decreasing stretch until quenching extinction is observed. This is primarily due to decreased heat transfer from the flame, while the magnitude of the losses remains the same. A unique local extinction flamelet phenomena and associated pre-extinction oscillations are observed at very low stretch. An ultimate quenching extinction limit is found at low stretch with sufficiently high induced heat losses.

Introduction

As humans expand into space and onto other planetary bodies, we need to understand how to live and work in those environments safety, but without undue restrictions. In spacecraft, the atmospheric control system and local cooling fans within hardware racks produce low velocity flows which can impinge upon flammable materials and create low stretch environments around those materials. How materials burn in these environments, and how to test materials for fire safety in these environments are issues facing NASA today. The objective of this fundamental study of flame characteristics in low stretch environments is to improve the understanding of materials flammability testing in normal gravity as it applies directly to spacecraft environments.

The behavior of diffusion flames at very low stretch rate, as found in many microgravity flames, has not been often studied. Flame stretch is the logarithmic rate of increase of flame area with time, and the concept of flame stretch can be applied to to both curved flames or to flames in velocity gradients. Low stretch flames exist in flows with small velocity gradients or in geometries with little flame curvature. It used to be thought that vanishing stretch rate corresponds to infinitely large Damkohler number, where residence times are long compared to chemical reaction times, and are typically associated with robust flames. That this is not the case has been pointed out in a theoretical analysis where radiative loss is included[1]. With radiative heat loss, a flame can be quenched at small stretch rate. Thus the behavior of diffusion flames at small stretch rate can not be characterized by a Damkohler number alone; an additional

parameter such as a radiative loss parameter is required.

Foutch and T'ien [2] used the radiative loss as well as a densimetric Froude number to characterize the blowoff (small Da) and quenching extinction (large Da) boundaries in stagnation-point diffusion flames under various convective conditions. An important conclusion of this study was that the shape and location of the extinction boundary, as well as a number of important flame characteristics, were *almost identical* for the buoyant, forced, and mixed convective environments they modelled. This theory indicates it should be possible to understand a material's burning characteristics in the low stretch environment of spacecraft (induced by fans and crew movements) by understanding its burning characteristics in an equivalent Earth-based stretch environment (induced by normal gravity buoyancy). Equivalent stretch rates can be determined as a function of gravity, imposed flow, and geometry. A generalized expression for stretch rate due to mixed convection includes both buoyant and forced stretch, and is defined[2] as $a = a_f(1+ a_b^2/a_f^2)^{1/2}$. For purely buoyant flow, the equivalent stretch rate is $a_b = [(\rho^e-\rho^*)/\rho_e]\ [g/R]^{1/2}$ [2,3]. For purely forced flow, the equivalent stretch rate is characterized by either $a_f = 2U_\infty/R$ for a cylinder[2, 4], or $a_f=U_{jet}/d_{jet}$ for a jet impinging on a planar surface[5,6]. In the experiments reported herein, $a_f=0$ and the buoyant stretch is varied through R, the radius of curvature. The buoyant stretch rate could also be obtained through varying g, the gravity level. In this way the effect of partial gravity, such as those found on the Moon (1/6 g) or Mars (1/3 g) on material flammability can be examined at Earth's gravity through equivalence n of flame stretch rates.

While theory indicates that microgravity flame characteristics can be obtained through

proper scaling of normal gravity flames, very few experiments on low-stretch diffusion flames have been reported. For most common configurations and sample dimensions, the induced buoyant flow on Earth is too high to achieve the low stretch rates of interest. Ohtani et al. [7-9] conducted detailed experiments of the bottom surface combustion of cylinders and rectangular flat pieces of PMMA. Cylinders ranged from 2.5-7.5 cm in radius. Flat pieces ranged from 3-10 cm in characteristic length. Using a linear scale, the authors extrapolated the experimental results to zero burning rate to estimate an extinction limit dimension of 23.5-25 cm radius for cylindrical pieces, and 14-25 cm for flat pieces. They suggested that extinction would occur when the convective heat flux from the flame to the burning surface becomes comparable to the radiative heat loss from the surface.

Himdi [10], and Vantelon et al. [11,12] conducted experiments on the bottom surface combustion of flat PMMA disks of various diameter from 2-15 cm . Detailed species and temperature profiles were made for each size as well as for various external radiant flux levels. For samples larger than 8 cm in width, cellular flames were observed. They estimated an extinction limit dimension of approximately 20 cm for flat pieces. They also suggested that the balance between convection and radiation is controlling the burning. In none of these experiments was the actual extinction limit observed.

Flame spread microgravity experiments have been conducted at very low speed flow, which is similar to low stretch. Microgravity research [13-16] identified that a quenching extinction branch exists for thin fuels under low velocity flow conditions in the absence of

buoyant flow. Flame spread rates decreased with opposed forced air flow due to oxygen transport limitations[15] in the absence of buoyant convection, and the flames ultimately extinguished at very low velocity due to excessive heat losses (surface radiation etc.) relative to the reduced heat generation in these weakly ventilated flames[14]. The transition from blowoff to quenching was found to be the most favorable condition for opposed flow flammability at a given oxygen level, and the opposed forced flow velocity at transition was found to exist at lower than attainable flows in normal gravity for the thin fuels. This raises issues for fire safety in spacecraft in the areas of materials testing, fire prevention, and extinguishment .

Experiments

The approach in these experiments was to conduct low stretch experiments at normal gravity that simulate the low stretch microgravity environment of spacecraft. As such, the normal gravity experiments were conducted using a cylindrical flame configuration with PMMA fuel samples ranging in radius of curvature from 2.5 cm to 200 cm, in order to overlap existing experimental data at the small end and extend the data base to the quench limit at the large end. Air flow was provided purely by buoyancy. Cooling on the back surface of the samples was also varied to control solid-phase conductive losses. Since the flame is weakest at ignition because the in-depth temperature profile is not established, the extinction limit separate from an ignition limit could not be determined until a second parameter, the back surface temperature, was changed long after the ignition transient.

A concept of the experimental apparatus is shown in Figure 1. The fuel sample was hung from the ceiling to avoid flow disturbances from the support structure. The apparatus was enclosed in a large double layered screen cage to eliminate room drafts while allowing free flow of air around the sample. An exhaust vent was recessed in the ceiling above the sample to remove combustion products while minimizing disturbances to the natural convective stagnation point flow below the sample. Sample probes, cameras, thermocouples, and other diagnostics were introduced on cantilevered extension arms through small openings in the wire screens for minimal disturbance.

The central area of the support apparatus exposed the 20 cm x 20 cm curved fuel sample while the remainder of the apparatus was inert. This allowed for reasonably-sized flames while still providing the large radius required to establish low stretch rates. The range of stretch rates of interest is 2-16 sec^{-1}, which correspond to approximate radii of 2.5 - 200 cm. Humidity and temperature in the lab were held consistently at 55% relative humidity and 22° C by the lab air-handling system.

The plastic fuel used in this experiment is cast polymethylmethacrylate, or PMMA, $C_5H_8O_2$, an amorphous uncrosslinked thermoplastic polymer. The 20-200 cm samples were made from 2.4 cm thick Plexiglas®* G stock from the same batch. The 2.5 cm and 5 cm radius samples which were formed by halving a solid cast PMMA cylinder (Perspex CQ®*) due to the

** In no instance does the identification of commercial products by manufacturer's name imply endorsement by the National Aeronautics and Space Administration, nor does it imply that the particular product is necessarily the best available material.*

difficulty in forming such tight radii with the thick material. To form the larger radii (20-200 cm), samples were heated under infrared lamps for 90 minutes until rubbery-soft and pliable as they reached a forming temperature near 430 K. The hot samples were then placed within a specially fabricated wood mold with felt covers and press-shaped in the desired radius of curvature for the cylindrical sections. They were insulated within the mold and left to cool slowly to allow stress relaxation during the cooling process.

The samples were placed in a cut-out in an aluminum sheet shaped to provide the same curvature as the fuel samples. The aluminum sheet was at least 40 cm by 60 cm by 0.3 cm thick. A new aluminum support was fabricated for each sample. A high temperature silicone was used to seal the sample to the aluminum support in the overlap area. An ice bath was used to cool the back surface of some samples so that an isothermal boundary condition on this back surface could be maintained.

The fuel samples were ignited using a retractable propane array of 40 small gas jet diffusion flames. A mass flow meter measured the amount of propane used during the ignition process. Ignition times varied with radius of curvature from 1-15 minutes, with larger radii needing more time to ignite. The yellow propane flame array heated the sample, which began to make characteristic sizzling and popping sounds. A blue flame appeared beneath the surface amid the yellow sooty propane flamelets.

When the PMMA flame was established beneath the sample, the propane was turned off. The PMMA flame turned completely blue within seconds of the igniter deactivation. As the test progressed, the solid-phase temperature profiles developed, and a soot layer appeared between the surface and the blue flame.

Color CCD cameras were used to record the test. Regression rate, standoff distance, and flame thickness were measured from these images. Resolution of the flame images was 0.1 mm or better. An uncooled, temperature-compensated infrared radiometer with a Schmidt-Boelter thermopile sensor was used to record the total radiant loss from the flame and surface emissions during the experiment. The spectral range was 0.6-15 microns, and a viewfactor was determined for each test to convert the reading to W/cm^2 values.

Type K thermocouples recorded solid and gas-phase temperatures prior to and during tests. The thermocouple signals were conditioned and cold-junction compensated, and recorded every 6 seconds. Solid-phase thermocouples were 0.0127 cm OD bare wire type-K thermocouples embedded at various depths in the sample through predrilled and re-sealed holes in the sample. Accuracy of the solid phase measurements is estimated to be 20°C. Gas-phase thermocouples were sheathed ungrounded 0.025 cm outer (sheath) diameter type-K thermocouples cantilevered into the flame by a 2 axis positioning system along the axis of the cylinder to minimize conductive heat loss. No corrections to the measurements for radiation or conduction errors were made because the corrections vary throughout the flame zone and peak at the stagnation plane, where they are difficult to estimate. It will be argued below that the

conclusions would not change if a correction to the temperature measurements was applied. At the stagnation plane, the radiative loss is significant due to the absence of convective heat transfer to balance the radiative loss. The peak flame temperatures reported here, which are on the oxidizer side of the stagnation plane, are estimated to be up to 100 K too low due to this radiative loss at these low stretch rates.

Results

Flame Appearance

One-dimensional stagnation point flames blanketed samples of 2.5, 5, 20, 50, and 75 cm (uncooled) radius of curvature. The blue-rimmed sooty flame for 5 cm radius samples, is shown in Figure 2a. Many vapor jets disrupted the flame surface at any given time. These vapor jets were due to surface rupture of vapor bubbles observed to form within the PMMA sample as it softened, swelled, and pyrolyzed. Vapor jets extended well beyond the blue outer flame, although no dripping was observed.

For the twenty cm radius sample, the flame was strongly sooting (see Fig. 2b) after the ignition transient, but vapor jet disruption was reduced as compared to the 5 cm radius flames. At approximately 15 minutes, the sample began to drip flaming molten drops of PMMA through the flame zone. The dripping increased with time, making measurement of the surface location increasingly difficult. Molten droplets disturbed the flame locally as the flame adjusted its height around the hanging droplet as well as during the actual dripping process.

The flames established over 50 cm samples (Figure 2C) were nearly all blue and blanketed the sample after the ignition transient. Vapor jet disruptions were minor. The only sooting noted during this test was localized around the droplets suspended from the burning surface. As the test proceeded, droplet formation and dripping became more frequent (although not as much as the 20 cm sample), and the amount of sooting increased.

Only without ice-bath cooling could 75 cm samples develop the one-dimensional uniform flames shown in Figure 2d. After ignition, the resulting flamelets grew and merged gradually over time as the solid-phase heating progressed, so that a blue uniform flame blanketed the surface was established by approximately 40 minutes. Yellow soot luminosity increases from 45 minutes until 55- 65 minutes. Beyond 65 minutes, dripping becomes more severe. Surface and flame locations become difficult to measure consistently by 100 minutes due to the uneven surface and associated flame distortions. Soot luminosity seems to decrease as well at about this time. In addition, the onset of flamelet behavior was observed at approximately 90 minutes due to an increase in regression-induced conductive losses.

For ice bath-cooled samples of 75 cm, 100, and 200 cm, multidimensional flamelets were observed throughout the test, in contrast with a one-dimensional flame blanketing the surface. Flamelets are a unique new near-limit low stretch flame adaptation observed for the first time in this geometry. Quenching extinction was observed for the 200 cm sample for back surface cooling via dry ice, where the dry ice was added after the ignition transient was complete.

The detailed one-dimensional flame data, taken during the pseudo-steady period where flame standoff was constant, is summarized in Olson[3]. The onset of the pseudo-steady period is defined as the time when the fuel heatup and molten PMMA swelling transients (≈30-60 minutes) were finished, and steady regression is observed. Due to the finite thickness of the samples, the pseudo-steady period ends with the regression transient, which is after regression of a sufficient fraction of the material, so that solid-phase conduction increases. Thus the flame was at its minimum heat loss during the pseudo-steady period.

Surface Regression Rates

Surface regression was measured two different ways in these experiments. The average surface regression measurements were based on the mass loss measurements (corrected for any mass loss through dripping), and are an average throughout the test. Local surface regression measurements (V_{regr}) are based on measurements of surface location as a function of time from the video during the experiment. The two compared favorably throughout the range of radii studied, and are plotted in Figure 3, along with other published data at higher stretch rates.

Stretch rates for Fig.3 were calculated from the experimental measurements. The stretch rate is defined in Eqn. 1 [2]. For these experiments, T^* ranged from 990 K to 865 K, and a ranged from 1.8-11.9 sec^{-1}.

$$a = \left[\left(\frac{T^* - T_e}{T^*}\right)\frac{g}{R}\right]^{\frac{1}{2}} \quad (1)$$

Figure 3 captures the surface regression rates for PMMA over the full range of flammability in air, from blowoff at high stretch, to quenching at low stretch. The solid line drawn through the central portion of the data ($3<a<100$ s^{-1}) has a slope of unity, which indicates $V_{regr} \propto a$. Infinite kinetics theory and experiments find a square root relationship[14] between regression and stretch at high stretch rates, but kinetics become important at low stretch rates and the dependence on flame stretch becomes stronger. This figure assumes the existence of a direct relationship between forced stretch [17], and buoyant stretch [9], and the excellent correlation between these different methods of stretch generation shows that this assumption is reasonable.

Ohtani et al [8] plotted their data on a linear scale (regression rate vs $(2R)^{-1/4}$) and extrapolated their results to zero regression rate (they never observed extinction) to estimate the radius of curvature at extinction would be around 25 cm. For a non-zero regression rate at the limit, the radius at extinction would be even smaller. This paper describes uniform flames well beyond their extrapolated limiting size, and a new flamelet phenomena encountered at small stretch extends the limit further. Quench extinction of low stretch flames was observed experimentally for the first time in normal gravity.

In Figure 3, the stretch rate below which uniform flame burning was not achieved is 3 s^{-1}, where departure from the linear correlation occurs. Similarly, the overall extinction limit is marked simply as a Quench limit, which means that flames could not sustain at these large radii (low stretch rates). In the low stretch region between these limits, a new flamelet phenomenon is observed, which is believed to be a new regime of near-limit unstable flame behavior which

occurs at low stretch. More detail on low stretch flamelets is reported in Olson [3].

The non-dimensional mass burning rate, $-f_w$ [17], is evaluated using

$$-f_w = \dot{m}''[\frac{2}{\rho_e \mu_e a}]^{\frac{1}{2}} \quad (3)$$

These data are plotted against stretch rate in Figure 4, using Eqn. (3). The non-dimensional burning rate decreases non-linearly with decreasing stretch in the low stretch regime. The flamelet regime and the overall Quench limit are at a stretch rate of 3 sec^{-1} at $-f_w = 0.3$, and 1.5 sec^{-1} at $-f_w \approx 0.15$, respectively. This is in good general agreement with predictions [2], where the non-linear trend is captured and the one-dimensional quench limit is predicted at 1.5 s^{-1} at $-f_w=0.3$.

Flame Structure Variations with Stretch

Video images of the experiments were analyzed frame by frame for surface location, outer blue flame boundary, and inner blue flame boundary. A typical set of measurements are shown in Figure 5 for a 50 cm radius of curvature sample. The above local burning rates were derived from the slope of the regressing surface. The outer blue flame standoff distance is measured from the regressing surface to the outer blue flame boundary, while flame thickness is the difference between inner and outer blue flame boundaries.

For the case shown in Figure 5, the ignition transient lasts for approximately 15 minutes before pseudo-steady flame standoff distances and surface regression was observed. The swelling of the surface during ignition is believed to be due to the development of a bubble layer within the solid as the in-depth thermal profile develops.

The visible flame thickness, distance of the T_{max} from the surface (derived from the temperature profiles discussed below), and outer blue standoff distance are plotted as a function of stretch rate in Figure 6. Flamelet information is only approximate because of inherent fluctuations in the flamelet behavior. The flame standoff distance and flame thickness increase substantially at low stretch. At sufficiently low stretch (3 sec^{-1}), the flame is unable to sustain a uniform, one-dimensional flame so far from the surface with such a diffuse reaction zone. The flame breaks up into smaller, thinner, three-dimensional flamelets that stabilize closer to the fuel surface. As stretch is reduced further, however, the flamelet standoff and thickness grow again and extinction of these flamelets occurs.

Local flamelet quench and complete Quench both occur as the flame zone thickness grows to approximately 2 mm and as temperatures drop to around 1100 K. The thickening of the flame zone is indicative of a slowing of the gas-phase reactions at these reduced temperatures, and this near-limit thickness and temperature may be indicative of a limiting reaction rate (heat release rate) below which the flame cannot be sustained for this system. Residence times increase inversely with stretch rate, but reaction times increase exponentially with decreasing temperature. Based on the measured flame temperature, the ratio of residence

time to reaction time decreases at low stretch, although the Damkohler number, typically defined at a fixed reference temperature, increases.

Temperature Profiles

The temperature profiles are non-dimensionalized using [2] non-dimensional temperature and non-dimensional distance as

$$\theta(\eta) = \frac{T(\eta)}{T_e} \tag{4}$$

$$\eta = \frac{ax}{2\sqrt{\int_0^x \rho_e \mu_e a x dx}} \int_0^y \rho dy \approx \frac{\sum_0^y \rho \Delta y}{\sqrt{\frac{2\rho_e \mu_e}{a}}} \tag{5}$$

The experimental temperature distributions were used to evaluate the integral by applying the ideal gas law for air density. Note the non-dimensional distance depends on the temperature field.

Figure 7 shows the five non-dimensional profiles obtained for one-dimensional flames. At stretch rates of 16.2 and 11.7 sec^{-1}, the non-dimensional temperature fields are non-dimensionally broader and cooler than at 5.9 sec^{-1}, which is the (non-dimensionally) narrowest and hottest of the four. As stretch is reduced from that point, the profile again becomes wider and cooler.

These non-monotonic trends in peak non-dimensional temperature and non-dimensional distance η_{Tmax} are captured in Figure 8. The data indicate that there is a maximum temperature somewhere between 5 and 11 sec^{-1}, and it is estimated from the locally weighted regression curvefit that the maximum occurs at approximately 6-7 sec^{-1}. η_{Tmax} mirrors this trend, with the smallest value at a similar curvefit estimate of 6-7 s^{-1}. The non-monotonic non-dimensional standoff distance η trend is different from the dimensionally increasing standoff distance trend with decreasing stretch. The temperature dependence of η is believed to be responsible for the difference in trends, where η is found to mirror the temperature trend. Low stretch theory [1] and the data of Figure 11 (presented later) indicate the temperature maximum corresponds to a transition from the blowoff to the quenching side of the flammability map. The locally-weighted regression curvefit values of 6-7 sec^{-1} for this transition is in good quantitative agreement with predictions[1,2,18].

Solid-Phase Temperatures

Embedded thermocouple data were used to reconstruct solid-phase temperature distributions during the experiment. An example of the raw temperature-time data is shown in Figure 9 for the 75 cm no ice-case.

The surface temperature is 630 K in Figure 9. As each thermocouple approached the surface, fluctuations were observable in the traces due to the liquid/bubble layer and associated material non-uniformities. As the bead entered the gas-phase, the fluctuations became very

strong. These fluctuations were due to vapor jetting and dripping [19,20]. Although not shown here, abrupt shifts in the temperature traces occurred in some runs due to thermocouple wire slipping and relaxation motions through the glassy layer. The transition from condensed phase to gas phase was at times difficult to discern due to dripping and sporadic wetting of the thermocouple. Due to swelling of the sample during the ignition transient, the initial thermocouple locations needed to be corrected for the observed swelling as well as regression in the construction of temperature profiles in the solid.

An example of the temperature profiles in the solid-phase is shown in Figure 10. The surface gradient is determined from this data at the same time as the gas-phase data taken in the previous section. In this way, errors in the surface energy balance (below) were minimized. For this 20 cm radius case, the near-surface profile appeared to reach a pseudo-steady state at 1000-1200 seconds, with a gradient at the surface of 24.0 K/mm.

Because of the finite thickness of the sample, the solid phase was never truly steady. Heat losses into the interior decayed with time during the heatup transient, but heat losses increased at later times with surface regression. This can be seen in Fig. 10, where the profiles steepen in response to regression at later times (thickness decreases from 25->22 mm). This decrease and later increase in heat losses correlated with the observed, uncooled 75 cm radius flame transitions from post-ignition flamelets to a uniform flame and later back to flamelets. These measured, time-resolved, solid-phase gradients agreed well with a transient numerical model of the solid [3].

Surface Energy Balance

The burning rate data and temperature measurements were used to evaluate each term of the surface energy balance at the solid surface, written as

$$\lambda_g \frac{\partial T_g}{\partial y} + q''_{rad} = \lambda_s \frac{\partial T_s}{\partial y} + \dot{m}'' L_v + \epsilon\sigma(T_s^4) \qquad (6)$$

The first term on the left-hand side is the conductive heat flux to the surface, the second term on the left is the net flame radiative flux absorbed by the solid (radiative influx minus reflected and transmitted flux). The first term on the right-hand side is the conductive heat flux into the solid interior, the second term is the energy needed for pyrolysis of the solid, and the last term is the surface radiative loss.

This model does not account for many known experimental complexities, such as the influences of the bubble layer and sample swelling on solid-phase temperature profiles, the changes in the material properties at the glass transition, the temperature-dependent properties, or the radiative absorption in-depth. Nevertheless, it does provide insight into the overall behavior of these flames. The values for each term for each stretch rate are given in Table 1. A detailed description of the data used to compute the various terms in this balance can be found in Olson [3]. The gas-phase temperature gradients at the surface were calculated using a second order regression of the gas-phase temperature profile data inside the peak temperature and

evaluating the slope of that fit at the surface. Solid-phase surface temperatures and the gradients at the surface were evaluated as discussed above. The measured burning rates were used. The q''_{rad} term, which was not directly measured, was computed to balance the above equation. The emissivity used is ϵ=0.85, based upon comparison of the measured surface temperatures and radiometer data from surface emissions. It is close to the value of 0.9 used in Yang and T'ien[15].

Figure 11 plots these terms as a function of stretch. The energy used for vaporization decreases with burning rate as stretch is reduced. The surface radiative loss term is effectively constant since the surface temperature was the same in all runs to within the error of the measurement. The rate of in-depth conductive heat loss is also fairly constant for the one-dimensional flames, with flamelets having slightly higher heat losses due to the incomplete coverage of the fuel surface.

Gas-phase conduction to the fuel surface reached a local maximum around the stretch rate of 6-7 sec^{-1}, consistent with the peak temperature and minimum non-dimensional standoff distance (η_{Tmax}) at the transition from the blowoff branch to the quenching branch (see again Fig. 8). The small levels of conductive (convective) flux from the flame at lower stretch rates(< 1 W/cm^2) are due to large flame standoff distances and reduced flame temperatures, which are typical of many flames in a reduced gravity. The gas-phase radiation to the surface, which is solved for to balance Eqn. 6, mirrors the gas-phase conduction. The decreasing net flux, which is the sum of conduction and radiation from the gas to the solid (●) in Figure 10, decreases in parallel with decreasing fuel vaporization, and it is a key factor in flame strength.

Based on the trends in Fig. 8 and Fig. 11, the flame appears to be able to adjusts its standoff distance in order to maintain the needed net heat flux. Thus the sooty one-dimensional flame at 3 s^{-1} (uncooled back), provides more radiative feedback than the non-sooty flamelet at $3s^{-1}$ (cooled back), and thus has a larger non-dimensional standoff distance η (and larger dimensional standoff distance as in Figure 6), so provides less gas-phase conductive feedback than its non-sooty counterpart. This observation is consistent with results from a sounding rocket experiment (DARTFire)[21], where the effect of a 1 W/cm^2 external radiant flux was to move the flame away from the PMMA surface to maintain the same net heat flux and subsequently the same spread rate.

The radiation exchange in these experiments is extremely complex. Transient sooting occurs at low stretch, and in-depth absorption and possible emission of the transmissive fuel contributes to the distributed thermal degradation noted in the samples, with the most transmissive sample showing the densest bubble layer [3]. Diffusion flame non-symmetries in the spectral gas-phase species' distributions also cause uncertainties in interpreting radiation measurements made on one side of the flame with energy balances made on the other. The spectral interactions of the radiating solid with the thick layer of radiatively-active hot monomer and soot in the gas-phase is not understood. More study of the radiant exchange in low stretch diffusion flames is needed.

To determine overall trends, the terms of the surface balance are compared as ratios. The ratio $F_{reutilization}$, is the fraction of gas-to-surface net heat flux used to vaporize more fuel, and another ratio, F_{loss}, is the fraction of gas-to-surface net heat flux that is lost to the solid interior and radiated from the system. In this way, $F_{loss}+F_{reutilization}=1$. ϕ, the fraction of gas-to-surface net heat flux that is conducted in depth, is defined for comparison with Yang and T'iens' theory [18].

$$F_{reutilization} = \frac{\dot{m}'' L_v}{\lambda_g \frac{\partial T_g}{\partial x} + q''_{rad}} \tag{7}$$

$$F_{loss} = \frac{\lambda_s \frac{\partial T_s}{\partial x} + \varepsilon\sigma(T_s^4)}{\lambda_g \frac{\partial T_g}{\partial x} + q''_{rad}} \tag{8}$$

$$\phi = \frac{\lambda_s \frac{\partial T_s}{\partial x}}{\lambda_g \frac{\partial T_g}{\partial x} + q''_{rad}} \tag{9}$$

These ratios are plotted in Figure 12 as a function of stretch rate, using the data in Table 1. They represent the pseudo-steady period for the one-dimensional flames and typical values for the flamelets.

Fractional heat losses increase as flame stretch is reduced. At the onset of flamelets at $3s^{-1}$, only 15% of the net heat flux is reused to vaporize more fuel; 85% of it is lost. At the Quench limit, only 10% of the heat flux is reused; 90% of it is lost. The value of ϕ at the Quench limit

of a=2 s^{-1} agrees well with the value of ≈0.45 predicted by Yang and T'ien [18] for the same stretch rate in air. It is interesting to note that over the range of stretch rates studied, that in-depth solid-phase losses are comparable to surface radiative losses.

The fractional losses are increasing at low stretch, but the losses themselves are not increasing, but actually remain fairly constant over the range of conditions studied. Instead, the net heat flux from the gas-phase to the surface decreases dramatically with decreased stretch, as shown in Fig.11. What changes significantly is the heat release in the gas phase - the reaction rate is decreasing. The limiting factor in the reaction rate is hypothesized here to be the oxygen transport to the flame in this low stretch (low convective) environment, just as it was hypothesized in low velocity flame spread [15]. Flamelet phenomena at very low stretch, where the flame breaks up into pieces and becomes multi-dimensional, is viewed as the flame's method of enhancing oxygen flow to the flame, through increased local curvature (stretch).

Conclusions

Experiments on buoyant low stretch stagnation point diffusion flames over a solid fuel (PMMA) cylinder were conducted over a range of radii from 2.5-200 cm, or 2-16 sec^{-1} stretch. These experiments were the first conducted in normal gravity at such low stretch for a large-scale solid fuel.

The results are consistent with characteristics of low-gravity, low-stretch flames. The only clear gravitational effect noted was the fuel dripping, which was inconvenient but did not change the overall trends provided by the experiment.

The surface regression rates and non-dimensional mass burning rates decreased monotonically with stretch rate in agreement with model predictions [1,2]. Overall mass burning rates and local regression rates agreed very well, and exhibited a linear dependence on stretch rate except near the limits. The low stretch surface regression rates extend the data base for PMMA to quenching extinction, so data is now available from blowoff to quenching.

Gas-phase temperature profiles showed a non-monotonic trend with stretch rate, where a maximum flame temperature and minimum non-dimensional standoff distance is found at a stretch rate of approximately 6-7 sec^{-1}. This maxima and its stretch rate were in good agreement with theoretical predictions [1,2] for a transition from the blowoff side of the flammability map to the quenching extinction side.

Solid-phase temperature measurements were in good agreement with simple models of the solid phase [3]. The time between ignition and the establishment of a uniform flame agreed well with the predicted solid-phase heating times. The later transition to flamelets correlated with increased conductive losses with sample regression.

Visible flame standoff distance and visible flame thickness were found to dimensionally

increase as stretch rate is decreased. Non-dimensionally, however, the standoff distance showed a non-monotonic trend, mirroring the gas-phase temperature trend due to its temperature dependence.

A surface energy balance was made using measured values of each term in the surface equation except gas-phase radiation, which was derived to balance the equation. The results of this balance indicated that, although heat losses remain relatively constant (surface radiative loss and in-depth conduction), the flame feedback to the solid (gas-phase conduction and flame-to-surface radiation) decreased dramatically with flame stretch. The ratio of the fairly constant losses to decreased heat feedback thus increases to the point at which the flame can no longer sustain itself, and quenching extinction is observed.

The limiting factor in the heat feedback is hypothesized to be small chemical heat release rates due to small oxygen-transport rates, similar to that previously observed in very low velocity flow flame spread phenomena. The new flamelet phenomena (multidimensional flames) extend the material flammability beyond the one-dimensional flame extinction limit by creating local flame curvature - increasing the flame surface area which equates to increased local flame stretch rate. The increased flame surface area provides for increased local oxygen flux to the flame.

These experiments support the theory that low gravity flame characteristics can be generated in normal gravity through proper use of scaling. Based on this work, it may be

feasible to apply this concept toward the development of an earth-bound method of evaluating materials flammability in various gravitational environments from normal gravity to microgravity, including the effects of partial gravity low stretch rates such as those found on the Moon (1/6g) or Mars (1/3g).

References

[1]T'ien, J.S., 1986; *Combustion and Flame*, Vol. 65, pp. 31-34.

[2]Foutch, D.W., and T'ien, J.S., 1987; *AIAA Journal*, Vol. 25, No. 7, pp. 972-976.

[3]Olson, S.L.; 1997; *Ph.D. Dissertation*, Case Western Reserve University.

[4]Tsuji, H., "Counterflow Diffusion Flames", *Prog. Energy Combust. Sci.*, V. 8, pp. 93-119, 1982.

[5]T'ien, J.S., Singhal, S.N., Harrold, D.P., and Prahl, J.M., "Combustion and Extinction in the Stagnation Point Boundary Layer of a Condensed Fuel", *Combustion and Flame*, Vol. 33, pp. 55-68, 1978.

[6]Pellett, G.L. et all "Velocity and Thermal Structure and Strain-Induced Extinction of 14 to 100% Hydrogen-Air Counterflow Diffusion Flames". *Combustion and Flame*, V. 112, pp. 575-592, 1998.

[7]Ohtani, H., Hirano, T., and Akita, K., 1981; *Eighteenth Symposium (International) on Combustion*, The Combustion Institute, pp. 591-599.

[8]Ohtani, H., Akita, K., and Hirano, T., 1982; *Journal of FIRE and FLAMMABILITY*, Vol. 13, pp. 203-214.

[9]Ohtani, H., Akita, K., and Hirano, T., 1983; *Combustion and Flame*, Vol. 53, pp. 33-40.

[10]Himdi, A.; 1983; *Thèse Docteur de Troisieme Cycle Enêrgetique*, Université de Poitiers.

[11]Vantelon, J.P., Himdi, A., and Gaboriaud, F., 1987; *Combustion Science & Technology*, Vol. 54, pp.145-158.

[12]Vantelon, J.P. and Souil, J.M.; 1987," *Combustion Science & Technology*, Vol. 54, pp.159-175.

[13]Olson, S.L.; 1987; NASA TM 100195, *MS Thesis*, Case Western Reserve University.

[14]Olson, S.L., Ferkul, P.V., and T'ien, J.S.,1989; *Twenty-Second Symposium (International) on Combustion*, The Combustion Institute, pp. 1213-1222.

[15]Olson, S.L.; 1991; *Combustion Science and Technology*, 76,4-6, pp. 233-249.

[16]Kashiwagi, T., McGrattan, K.B., Olson, S.L., Fujita, O. Kikuchi, M. And Ito, K.; 1996, *The Twenty-Sixth Symposium (International) on Combustion*, to appear.

[17]T'ien, J.S., Singhal, S.N., Harrold, D.P., and Prahl, J.M.; 1978; *Combustion and Flame*, Vol. 33, pp.55-68.

[18]Yang, C. T., and T'ien, J.S., 1997, Proceedings of the ASME National Heat Transfer Conference, HTD-Vol.341, Vol 3 - Fire and Combustion, pp. 131-138.

[19]Seshadri, K. and Williams, F.A., 1975; Chapter 5 of *Halogenated Fire Suppressants, ACS Series # 16*, Gann, D. ed., American Chemical Society, pp. 149-182.

[20]Seshadri, K. and Williams, F.A., 1978; *Journal of Polymer Science: Polymer Chemistry Edition*, Vol. 16, pp. 1755-1778.

[21]Olson, S.L., Altenkirch, R. A., Bhattacharjee, S., Tang, L., Hegde, U., "Diffusive and Radiative Transport in Fires Experiment: DARTFire", proceedings of the Fourth International Microgravity Combustion Workshop, Cleveland, OH, May 19-21, 1997.

NOMENCLATURE

a stretch rate, sec^{-1}

$a = a_f(1+ a_b^2/a_f^2)^{1/2}$ equivalent stretch rate

$a_b = [(\rho^e-\rho^*)/\rho_e]$ [g/R] buoyant stretch rate

$a_f = 2U_\infty/R$ forced stretch rate for a cylinder

$a_f = U_{jet}/d_{jet}$ forced stretch rate for a jet impinging on a planar surface

Da Damkohler number

d_{jet} diameter of the jet

F_{loss} fraction of heat feedback that is lost

$F_{reutilization}$ fraction of heat feedback used to vaporize more fuel

$-f_w$ non-dimensional fuel blowing velocity

g gravitational acceleration, 980 cm/s^2

L_v Latent heat of vaporization = 1700 J/g

$\dot{m}''$ mass burning rate, g/cm^2 sec

q''_{rad} radiant flux from gas absorbed at surface, W/cm^2

R radius of curvature, cm

T_e ambient temperature, K

T_{max} maximum flame temperature, K

T_s surface temperature, K

T_g gas temperature, K

T^* average temperature between T_{max} and T_s, K

T_η temperature at η, K

U_∞ forced flow velocity, cm/s

U_{jet} jet velocity, cm/s

V_{regr} surface regression rate, cm/s

x coordinate along surface of cylinder

y coordinate normal to the surface of the cylinder

ϵ emissivity of fuel surface= 0.85

η gas-phase non-dimensional distance

θ non-dimensional temperature

$\lambda_s = 2.09 \times 10^{-3}$ W/cm K @ 300 K , solid thermal conductivity

$\lambda_g = 5.77 \times 10^{-4}$ W/cm K @800K., gas thermal conductivity

μ_e ambient viscosity , 1.85×10^{-5} kg/m s for air

ρ solid fuel density, kg/m^3

ρ_e ambient air density, 1.176 kg/m^3

ρ^* air density at T^*

σ Stefan-Bolzman constant, 5.729×10^{-12} W/cm^2 K^4

Φ percent of heat flux to the surface that is conducted into the solid

Table 1
Surface Energy Balance

R, cm	a, sec^{-1}	$\lambda_g \frac{\partial T_g}{\partial x} + q''_{rad} = \lambda_s \frac{\partial T_s}{\partial x} + \dot{m}'' L_v + \varepsilon\sigma(T_s^4)$ (W/cm^2)				
2.5$^+$	16.2	1.385	1.948	0.52	2.04	0.77
5$^+$	11.7	0.91	2.24	0.63	1.75	0.77
20$^+$	5.9	1.21	0.66	0.5	0.59	0.77
50$^+$	3.6	0.83	0.81	0.52	0.36	0.77
75$^+$	2.9	0.54	1.21	0.73	0.26	0.77
75*	3	1.32	0.55	0.9	0.2	0.77
100*	2.5	1.21	0.55	0.84	0.15	0.77
200*	1.8	1.15	0.59	0.84	0.14	0.77

+ one-dimensional flames, during pseudo-steady period
* flamelets

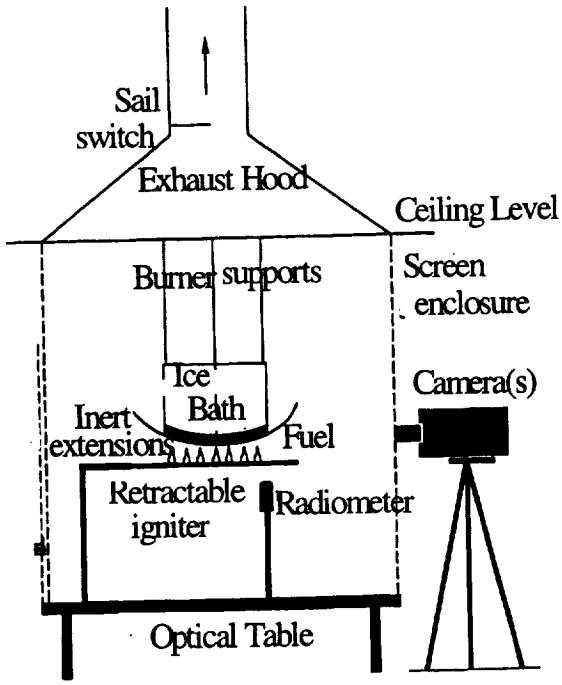

Figure 1 Experiment layout with fuel sample support apparatus suspended within hooded screened cage mounted on optical table.

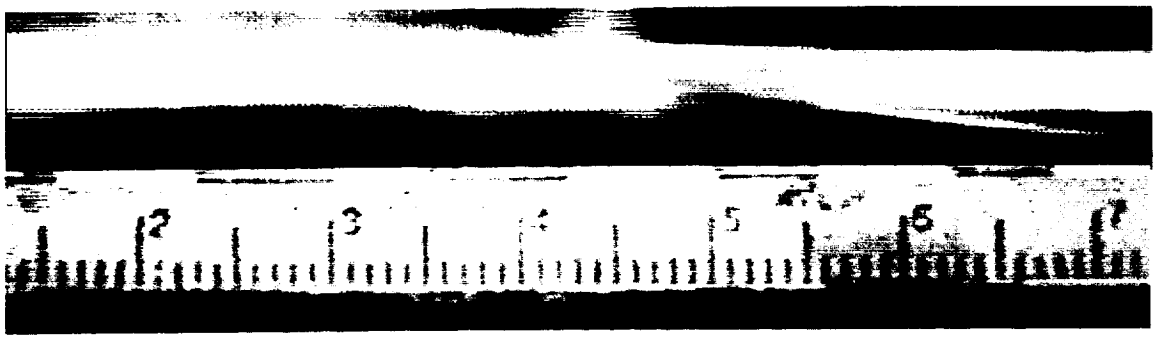

a) 5 cm radius flame and scale in mm.

b) 20 cm radius flame and scale in mm.

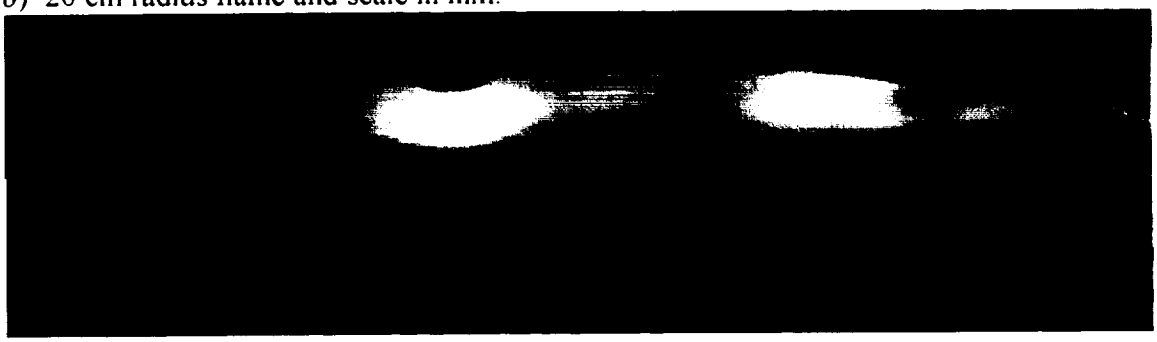

c) 50 cm radius flame and scale in mm.

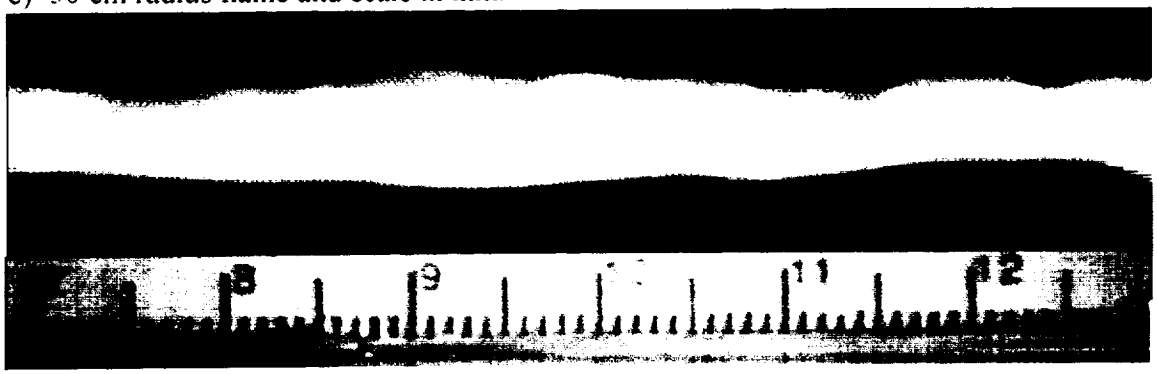

d) 75 cm radius flame and scale in mm.

Figure 2: side view of uniform flames at various radii of curvature.

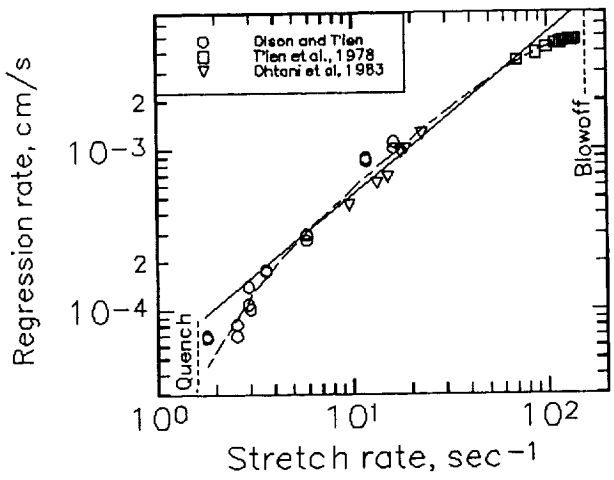

Figure 3: Surface regression rate measurements as a function stretch rate. Data spans from blowoff extinction at high stretch rate to quenching extinction at low stretch rate. Line through linear portion of data (away from limits) has a slope of unity.

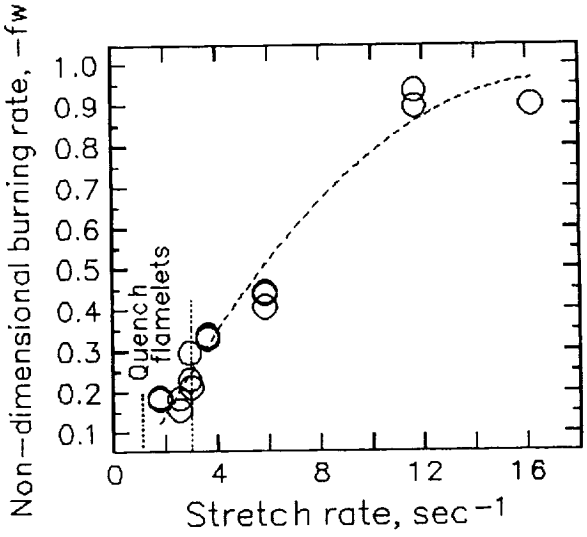

Figure 4: Non-dimensional burning rate as a function of stretch rate for the buoyant low stretch experiments.

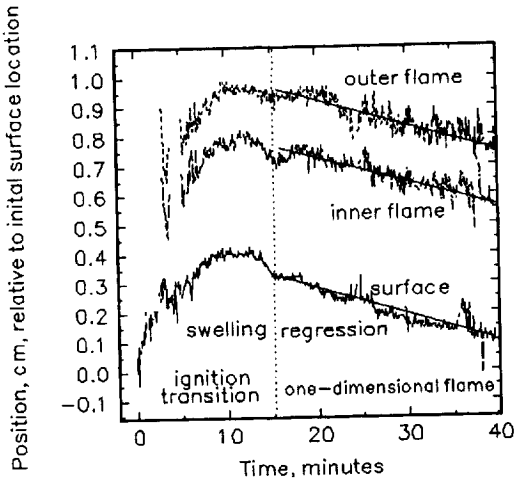

Figure 5: Measured surface and flame locations as a function of time during an experiment with a 50 cm radius of curvature sample.

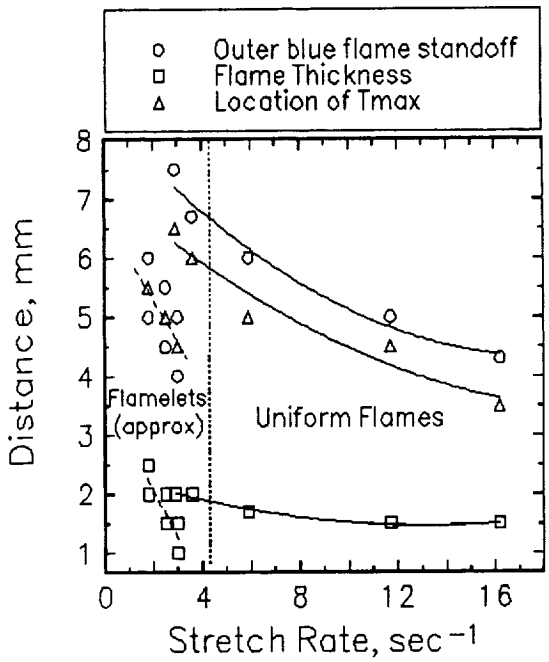

Figure 6: Flame structure information as a function of stretch rate.

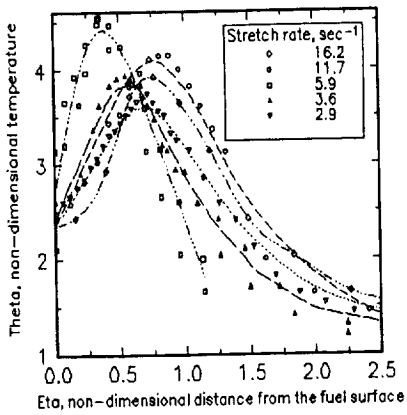

Figure 7: Non-dimensional temperature profiles for uniform flames from a stretch rates from 2.9-16.2.

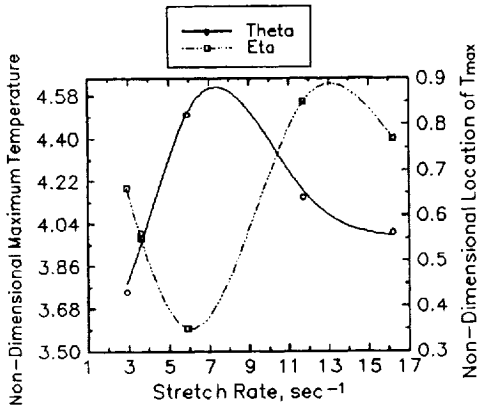

Figure 8: Maximum non-dimensional flame temperature and its non-dimensional location as a function of stretch rate for uniform flames.

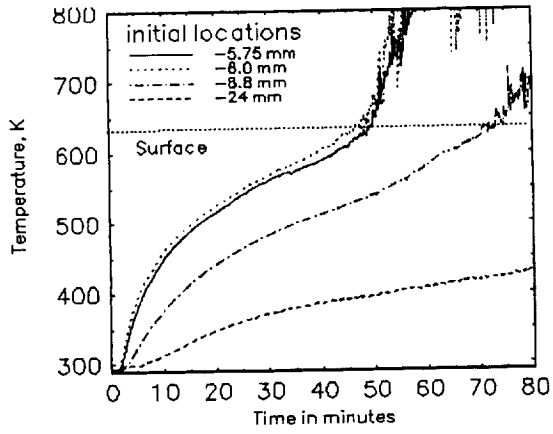

Figure 9: Solid-Phase temperature measurements as a function of time during the 75 cm no-ice experiment 16.

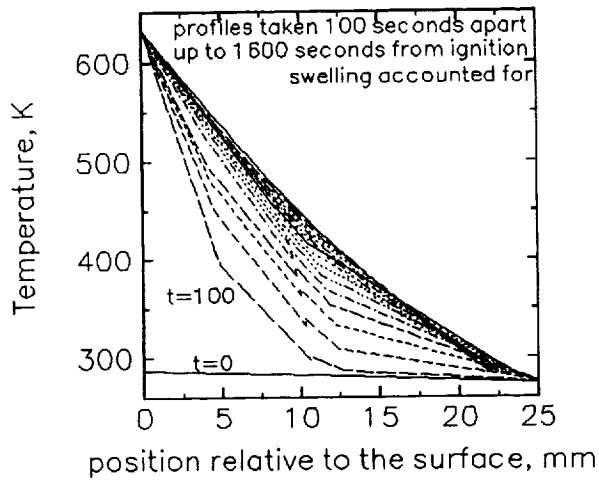

Figure 10: Reconstructed solid-phase temperature profiles as a function of time for a 20 cm sample.

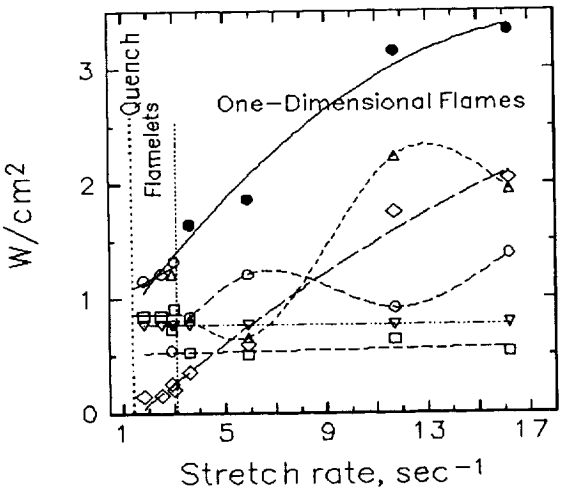

Figure 11: Surface energy balance terms in Equation 6, plotted as a function of stretch rate. □= solid conduction, ○=gas conduction, ◇=fuel vaporization, △= gas radiation, ▽= solid radiation, ●= net gas flux (conduction+radiation)

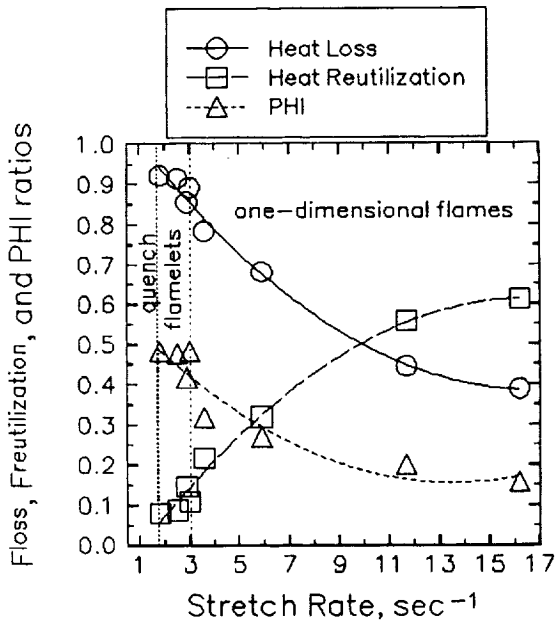

Figure 12: Loss, Reutilization, and PHI ratios as a function of stretch rate.